



PERGAMON

SCIENCE @ DIRECT®

International Journal of Rock Mechanics &amp; Mining Sciences ■ (■■■■) ■■■-■■■

International Journal of  
Rock Mechanics  
and Mining Sciences[www.elsevier.com/locate/ijrmms](http://www.elsevier.com/locate/ijrmms)

# Stress, instability and design of underground excavations

C.D. Martin<sup>a,\*</sup>, P.K. Kaiser<sup>b</sup>, R. Christiansson<sup>c</sup>

<sup>a</sup> *Department of Civil and Environmental Engineering, University of Alberta, Edmonton, Alberta, Canada T6G 2G7*

<sup>b</sup> *MIRARCO, Geomechanics Research Centre, Laurentian University, Sudbury, Ont., Canada*

<sup>c</sup> *Swedish Nuclear Fuel and Waste Management Company, Stockholm, Sweden*

Accepted 30 June 2003

## Abstract

When the stress-induced risks to a projects warrant it, in situ stress must be measured. However, as the stress-induced risks increase, i.e., the stress magnitudes approach the rock mass strength, the confidence in commonly used stress measurement techniques decrease. The design of underground openings at depth requires knowledge of the in situ stress state, yet it is for these design conditions where our confidence in stress measurement techniques is at its lowest. To quantify the stress state for these conditions, elements of the Observational Design Method have to be used. These elements rely on the development of a geological site model, documented observations of over stressed rock in pillars or near the boundary of underground openings, and iterative two- and three-dimensional numerical modelling calibrated with observations. Examples are provided to illustrate how the philosophy of Observational Design Method can be used to infer the in situ stress state.

© 2003 Elsevier Ltd. All rights reserved.

**Keywords:** In situ stress; Instability; Modelling

## 1. Introduction

Design of underground excavations requires an assessment of risk. While formal quantitative risk analysis is not routinely carried out in geotechnical engineering, elements of such risk analysis form the foundation of the Observational Design Method described by Peck [1]. Today the Observational Design Method often forms one element of the design process illustrated in Fig. 1. Inherent in this design process is the quantification of the anticipated range of values expected for any of the input design variables. In the design of underground openings the ratio of strength of the rock mass to the in situ stress state may be used as a simple index to assess the risk of overstressing the rock mass. The consequences of this overstressing depends on many factors, e.g., size and purpose of the opening, serviceability, etc. The designer must perform this risk assessment with or without the knowledge that the in situ stress data, which forms the corner stone of the analysis, may not be known with confidence.

Since the 1960s extensive efforts have been extended to develop stress measuring techniques. Today a number of tools exist to measure the two- and three-dimensional in situ stress state. The use of these tools and indirect observations have led to the development of the World Stress Map. Regionally, stress databases have been developed (e.g., for the Canadian Shield by Herget and Arjang [2] or the Scandinavian Shield by Stephansson [3]). While such information is useful in the early design stages of a project, if the risk to a project warrant it stress may have to be measured. When a stress measurement program is undertaken the designer must be aware that the result from such a stress measurement campaign cannot be defined by a single stress state but a range in a stress tensor. It must also be realized that for many situations associated with deep excavations, i.e., in deep mining, it may not be possible to measure the in situ stress state, e.g., because boreholes are no longer stable.

In this paper we highlight some of the recent findings from in situ stress measurement programs and how the variability in the in situ stress data can be managed when assessing project risks. Examples are also provided to illustrate how the philosophy of Observational Design Method can be used to infer the in situ stress state.

\*Corresponding author. Tel.: +1-780-492-2332; fax: +1-780-492-8198.

E-mail address: [dmartin@civil.ualberta.ca](mailto:dmartin@civil.ualberta.ca) (C.D. Martin).

Nomenclature	
$\sigma_{ci}$	laboratory intact uniaxial compressive strength
$\sigma_{cm}$	rock mass uniaxial compressive strength
$\sigma, \sigma_2, \sigma_3$	principal stresses
$\sigma_H, \sigma_h, \sigma_v$	maximum horizontal, minimum horizontal and vertical stress
$\sigma_{NN}, \sigma_{EE}, \sigma_{UU}$	stress component in the North, East and Up directions.
$\bar{G}$	mean stress tensor
$\sigma_{max}$	maximum tangential stress around underground opening
$\gamma$	unit weight of overburden
$D$	depth
$k$	stress ratio
$E_m$	deformation modulus
$\tau$	shear strength
$c$	cohesion
$\sigma_n$	normal stress on a plane
$\phi$	friction angle
$SL$	stress (tangential) level around boundary of underground openings
$GSI$	geological Strength Index
$d_f$	depth of stress-induced failure
$\Delta_{RE}$	released strain energy
$COV$	coefficient of variation
$\mu$	statistical mean
$\sigma$	statistical standard deviation
SKB	Swedish Nuclear Fuel and Waste Management Company
AECL	Atomic Energy of Canada Limited
Äspö	HRL SKB's Äspö Hard Rock Laboratory Sweden
URL	AECL's Underground Research Laboratory Canada

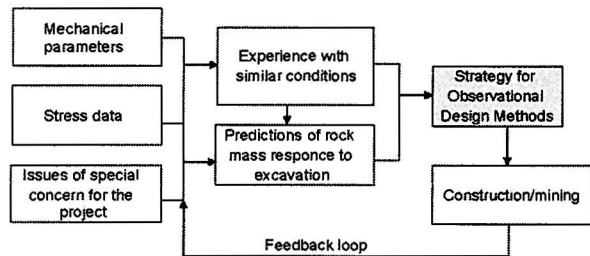


Fig. 1. Design of underground excavations in rock.

## 2. Stress and stress determination

As discussed elsewhere in this Issue, there are many methods to determine stresses. A listing of those techniques commonly used is included in Table 1. It should be noted that for deep excavations the large-scale back analysis methods often provide the more reliable results. In this section we review the presentation of data from these methods.

Mathematically, the stress tensor is a second-order Cartesian tensor with nine stress components. Three stress components that are perpendicular to the planes are called normal stresses. Those components acting tangent to these planes are called shear stresses. On engineering projects the directions for the in situ stresses are expressed in terms of a Trend (Azimuth) and Plunge (Dip) related to compass coordinates. Trend and Plunge are reserved for lines or vectors as opposed to using Dip and Dip Direction used to express the attitude of planes. A general right-hand coordinate system for describing the stress tensor, i.e., compass coordinates, could be East–North–Up or North–East–Down as illustrated in Fig. 2.

Once stress measurements have been carried out the results are often presented in the form of the example given in Table 2. To determine the mean stress from a series of stress measurements, the measurements must first be expressed in a common coordinate system such as indicated by Fig. 2. This must be carried out for each stress tensor to be averaged. The mean stress tensor  $\bar{G}$  for  $n$  stress measurements can then be found by [4]

$$\bar{G} = \begin{pmatrix} \frac{1}{n} \sum_{i=1}^n \sigma_{EE_i} & \frac{1}{n} \sum_{i=1}^n \sigma_{EN_i} & \frac{1}{n} \sum_{i=1}^n \sigma_{EU_i} \\ \frac{1}{n} \sum_{i=1}^n \sigma_{NE_i} & \frac{1}{n} \sum_{i=1}^n \sigma_{NN_i} & \frac{1}{n} \sum_{i=1}^n \sigma_{NU_i} \\ \frac{1}{n} \sum_{i=1}^n \sigma_{UE_i} & \frac{1}{n} \sum_{i=1}^n \sigma_{UN_i} & \frac{1}{n} \sum_{i=1}^n \sigma_{UU_i} \end{pmatrix}. \quad (1)$$

In Eq. (1) the subscripts refer to compass directions, e.g.,  $\sigma_{EE}$  refers to the stress component in the East direction. Having obtained the mean stress tensor, the mean principal stresses can be readily determined. A stereonet or the Dot product can then be used to check that the orientation of the three mean principal stresses are in fact perpendicular to each other, i.e., the Dot Product of orthogonal vectors is zero.

The orientation of the principal stresses are often shown on a stereonet. Fig. 3 presents the orientation of the principal stresses from Table 2 and the computed mean principal stresses. Inspection of Fig. 3 illustrates the variability associated with stress measurements, particularly for  $\sigma_2$  and  $\sigma_3$  and the difficulty in presenting and interpreting the results. It is possible that published mean stresses have not been properly calculated, using Eq. (1), and this adds additional uncertainties when estimating stresses based on published databases.

Because of this variability, the most common question asked when undertaking a stress measurement campaign is “How many measurements must be taken to obtain a

Table 1  
Stress measurement techniques tried at AECL's Underground Research Laboratory summarized from Martin [42] and Martin et al. [45]

Method	Technique	
Indirect	Triaxial strain cells	Modified CSIR CSIRO Borre probe
	Biaxial strain cells	CSIR door stopper USBM gauge Borehole slotter
	Hydraulic fracturing	Maximum stress
	Hydraulic fracturing	Minimum stress
	Convergence	Martin et al. [46]
Large-scale back-analysis	Under-excavation	Wiles and Kaiser [7]
	Radial displacements	Read [47]

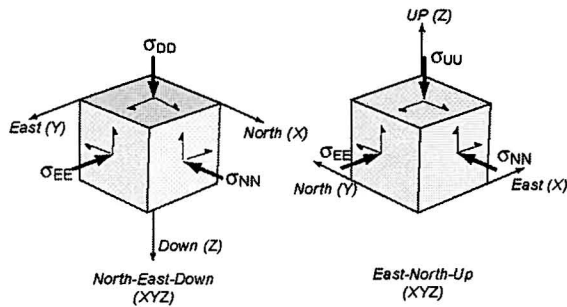


Fig. 2. General right-hand coordinate systems commonly used for describing the stress tensor in compass coordinates. In geomechanics compression is positive and positive shear stresses act in a positive direction on a negative face.

Table 2  
Example of 4 triaxial overcore test results presented as principal stresses

$\sigma_1/\text{Tr}/\text{Pl}$ (MPa/°/°)	$\sigma_2/\text{Tr}/\text{Pl}$ (MPa/°/°)	$\sigma_3/\text{Tr}/\text{Pl}$ (MPa/°/°)
33.1/237/25	18.9/339/23	16.2/106/55
26.3/238/17	14.5/136/36	7.9/349/49
33.1/233/29	17.0/142/02	14.7/049/61
34.1/244/09	18.8/145/45	13.0/324/44

reliable mean stress tensor?”. Unfortunately, there is no single or simple answer as it is directly related to the project risks. Wiles and Kaiser [5] analysed data from AECL's Underground Research Laboratory and concluded that 10 overcore triaxial measurements were needed before the mean could be statistically determined in sparsely fractured granite, assuming that the rock mass response was linear elastic. However, Martin et al. [6] showed that this number rapidly decreases as the volume of rock associated with the measurement

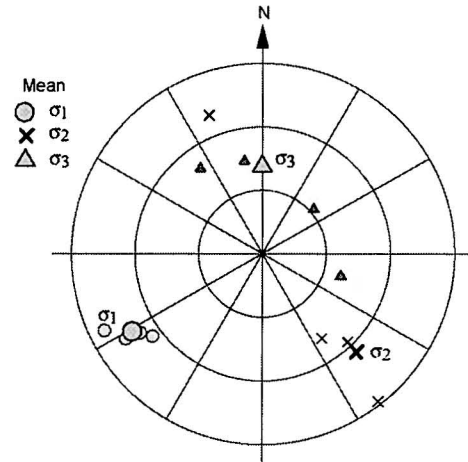


Fig. 3. Lower hemisphere stereonet showing the orientation of the principal stress and the mean principal stresses.

technique increases. For example, they showed that the in situ stress state determined by back analysis of convergence measurements gave the same values as the mean from 10 overcore measurements. Similarly, the Under-Excavation technique, developed by Wiles and Kaiser [7], is a back-analysis technique that involves a large volume of rock, in the order of 1000 m<sup>3</sup>, as compared to 1–5 m<sup>3</sup> by the other types of stress measurement techniques. In the authors' opinion, this technique has been undervalued in that it is not frequently enough utilized. Measurements made at the AECL's Underground Research Laboratory demonstrated, that a single measurement obtained using the Under-Excavation method produced a similar stress state as a large number of more conventional stress measurement tests [6].

### 3. Stress estimation from databases

During the preliminary design stages of a project it is often adequate to use stress information that has been accumulated on previous projects to estimate the regional stress state. Many countries have compiled stress data bases that are publicly accessible.<sup>1</sup> For example databases, including results from both over-coring and hydrofracturing measurements, have been established for both the Scandinavian [3] and Canadian Shield [2], extending to depths of 800 and 2500 m, respectively. These database are compiled from civil engineering and mining projects and are composites, gathered from a variety of geographical and geological conditions. Fig. 4 shows the distribution of stress measurements with depth in the Scandinavian Shield.

<sup>1</sup>The World Stress Map Project currently contains over 10,000 publicly accessible stress data sets [www.wsm.physik.uni-karlsruhe.de](http://www.wsm.physik.uni-karlsruhe.de)

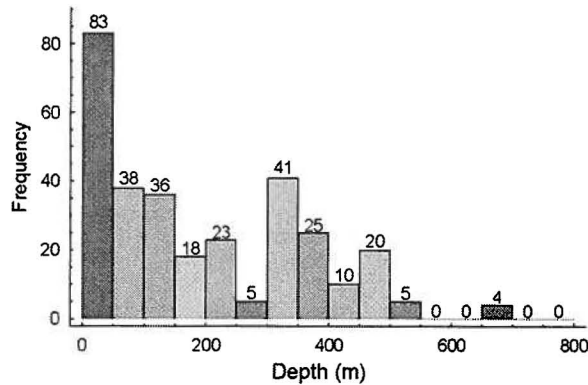


Fig. 4. Distribution of stress measurements with depth in the Scandinavian Shield.

Note that most of the measurements are located near the ground surface with few measurements at depths below 500 m. Hence using databases tends to predict in situ stresses at depth can be statistically challenging.

Stress data from triaxial stress measurements are usually reported in terms of the principal stresses  $\sigma_1$ ,  $\sigma_2$  and  $\sigma_3$  and their associated trend and plunge. However, in Scandinavia and Canada the major ( $\sigma_1$ ) and intermediate ( $\sigma_2$ ) principal stresses tend to be near horizontal (dip between zero and about  $10^\circ$ ) and the minimum principal ( $\sigma_3$ ) stress tends to be approximately vertical. Consequently, the maximum ( $\sigma_H$ ) and minimum ( $\sigma_h$ ) horizontal stress and the vertical ( $\sigma_v$ ) stress are used synonymously with  $\sigma_1$ ,  $\sigma_2$  and  $\sigma_3$ , respectively. The former notation ( $\sigma_H, \sigma_h, \sigma_v$ ) is adopted in this paper. This near coincidence between the principal stress directions and the horizontal and vertical should not be assumed at all project sites. In areas of significant topography, the principal stress directions could well be at completely different directions to the horizontal and vertical.

### 3.1. Vertical stress

The gravitational vertical stress at a depth  $D$  is the product of the depth and the unit weight ( $\gamma$ ) of the overlying rock mass. The unit weight of intact rock varies between 25 and 30 kN/m<sup>3</sup> for most common rocks such as granite, volcanics, metasediments, limestone, etc. Thus the vertical gravitational stress ( $\sigma_v$ ) is often estimated from the simple relationship:

$$\sigma_v = \gamma D \quad (2)$$

indicating that the overburden stress should increase linearly with depth ( $D$ ). Measurements of vertical stress at various mining and civil engineering sites supports Eq. (2) with the vertical stress gradient ranging from 0.025 and 0.030 MPa/m (see Table 3).

While the vertical stress tends to be on average equal to the weight of the overburden, the vertical stress can

Table 3

Summary of measured vertical stress gradients in various rock types

Vertical stress gradient (MPa/m)	Location (rock type)	Depth (m)	Reference
0.0249	Elliot Lake (Quartzites)	900	[48]
$0.0266 \pm 0.0028$	World data	0–2400	[49]
0.0270	World data	0–3000	[50]
0.0265	World data	100–3000	[51]
$0.026 \pm 0.0324$	Canadian Shield	0–2200	[52]
$0.0266 \pm 0.008$	Canadian Shield	0–2200	[53]
0.027	URL, Granite	0–440	[42]
0.0285	Canadian Shield	0–2300	[54]
0.0260	Canadian Shield	0–2200	[10]
0.0264	Åspö HRL, Diorite	150–420	[55]
$0.0249 \pm 0.00025$	Sellafield, UK (Sandstones/Volcanics)	140–1830	[56]

vary significantly from this trend. For example Martin and Chandler [8] showed that the vertical stress normalized to the weight of the overburden ranged from 1 to 3 (Fig. 5). They showed that this variation was caused by large-scale asperities along a fault, and that these asperities resulted in heterogeneous normal stresses acting on the fault. These stress perturbations influenced the vertical stress approximately 150 m below the fault. Hence, while the vertical stress can be estimated by the weight of the overlying rocks significant deviation from this mean should be anticipated and this deviation can be less than the weight of the overburden. Experience shows that these deviations are greatest close to the ground surface.

In the Scandinavian Shield, the coefficient of variation<sup>2</sup> for the linear relationship given Eq. (2) varies significantly with depth (Fig. 6). At depths greater than 500 m COV is less than approximately 20% but exceeds 100% at more shallow depth. Hence, while the mean vertical stress can be estimated by the weight of the overlying rocks, significant deviation from this mean should be anticipated, particularly close to the ground surface.

In the Canadian Shield at a depth of 2000 m, while the mean overburden stress would be expected to fall between 50 and 60 MPa depending on the rock density, the 90% confidence limits are 40–70 MPa. In other words, while there is in general a linear trend with depth for the vertical stress, values with a range of  $\pm 30\%$  must be anticipated. This range can only be narrowed by stress measurements or careful back-analysis.

### 3.2. Horizontal stresses in the Canadian and Scandinavian Shield

An example of the horizontal stress data contained in the database that was compiled from Swedish and

<sup>2</sup>Coefficient of variation (COV) = Standard deviation/mean  $\times$  100%.

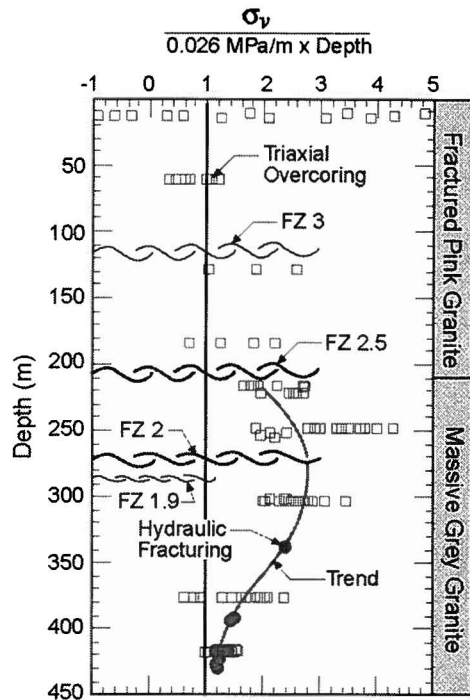


Fig. 5. The variation in vertical stress with depth measured at AECL's URL, modified from Ref. [8].

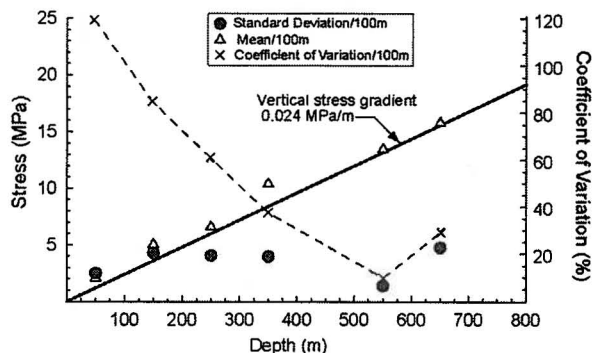


Fig. 6. Comparison of the average vertical stress gradient with the mean, standard deviation and coefficient of variation determined over 100 m intervals using the vertical stress from the Scandinavian Shield stress database.

Finnish stress measurements for the Scandinavian Shield is illustrated in Figs. 7a and c. The database contains 46 different boreholes with 418 measurements carried out in gneiss, granite and diorite. For comparison purposes, the horizontal stress data compiled by Herget and Arjang [2] from various hardrock mines to depths of 2200 m in the Canadian Shield is given in Figs. 7b and d. The stress databases from both the Scandinavian and Canadian Shield show a gradual increase in stress magnitude with depth, although there is considerable scatter in the measurements at any given

depth. Shown on Figs. 7a–d is the linear best fit to the data and a nonlinear best fit. The nonlinear best fits tends to predict lower stress magnitudes at depth compared to the linear trends. Inspection Figs. 7a–d provides the following:

1. Both the maximum horizontal stress and minimum horizontal stress magnitudes are larger in Canada than in Scandinavia
2. The minimum horizontal stress in Scandinavia is less than the vertical stress, whereas in Canada the minimum horizontal stress is greater than the vertical stress.

Provided in Figs. 7e and f is the ratio between the maximum horizontal stress and the minimum horizontal stress. In Scandinavia this ratio tends to vary approximately between 1 and 2, while in Canada it ranges between 1 and 2.5. Examination of the nonlinear fits to the data in Figs. 7e and f indicated that in fact the average ratios are very similar. One thing is clear from these figures; the variation in horizontal stress is far greater than what is observed in the vertical stress, particularly at shallow depths.

Since the 1980s site characterization programs for nuclear waste management programs in Canada, Finland and Sweden have established detailed stress profiles from the ground surface to approximately 1000 m depth. Christiansson and Martin [9] reported on the findings from the detailed site characterization programs carried out at SKB's Äspö Hard Rock Laboratory (HRL) and the Forsmark site in Sweden, as well as the AECL's Underground Research Laboratory (URL) in Canada. Fig. 8 presents a compilation of the maximum stress magnitude with depth measured at the URL, Äspö HRL and Forsmark. At these sites, the distribution of the maximum stress with depth does not follow the linear nor nonlinear trend suggested by Fig. 7. Inspection of Fig. 8 reveals that at all three sites the increase in stress magnitudes from the surface to between 200 and 300 m depth is gradual but that below this depth range the stress magnitude rapidly increases. At the URL and Äspö HRL the maximum stress magnitudes attained beyond 500 and 600 m depth appears to be independent of depth, at least for the next 200–400 m. In all cases the rapid increase in stress magnitude at depth correlates to the location of subhorizontal geological structures. At Äspö HRL the investigations into these structures is ongoing. At the URL the increase in magnitude is associated with a major thrust fault. Martin and Chandler [8] showed using numerical modeling that movement along the fault causing stress relief near the ground surface could explain the low stress magnitudes above the fracture zone. At present this appears to be a viable explanation for the stress relief at all three sites.



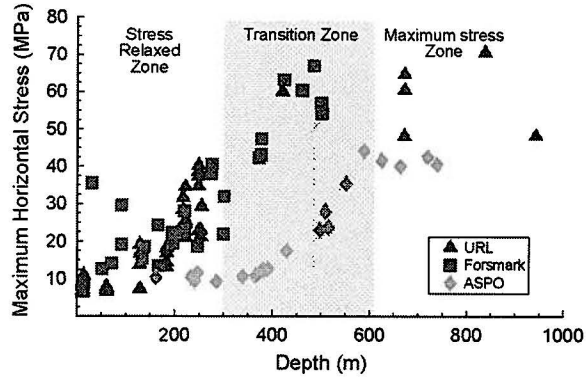
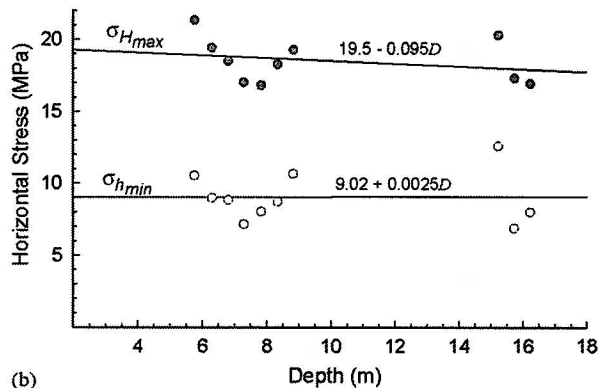


Fig. 8. Summary of the maximum stress magnitude versus depth measured at SKB's Äspö Hard Rock Laboratory and Forsmark SFR Facility in Sweden and AECL's Underground Research Laboratory in Canada. Note the rapid increase in stress between 300 and 500 m depth. Data from Ref. [9].



(a)



(b)

Fig. 9. A 'pop-up' observed at a quarry site in granite in Southeastern Manitoba and the horizontal stress determined using the USBM Borehole Deformation Gauge in a vertical borehole. (a) Quarry 'pop-up'. (b) Measured horizontal stress.

the crust and variation of elastic constants, density and thermal expansion coefficients through the crust and mantle. Sheorey's approach provides a simplified

equation which can be used for estimating the average horizontal to vertical stress ratio ( $k$ ):

$$k = \frac{(\sigma_H + \sigma_h)/2}{\sigma_v} = 0.25 + 7E_m \left( 0.001 + \frac{1}{D} \right), \quad (3)$$

where  $D$  (m) is the depth below surface and  $E_m$  (GPa) is the average deformation modulus of the upper part of the earth's crust measured in a horizontal direction. A plot of this equation is given in Fig. 11 for deformation moduli ranging from 10 to 75 GPa. Fig. 11 implies that at a depth of 500 m for example,  $k$  would be expected to range from approximately 0.5 to 2 provided the modulus ranged from 10 to 75 GPa.

A recently completed rock mechanics experiment was carried out at SKB's Äspö HRL [12]. The experiment investigated the range in deformation modulus that could be expected between 400 and 500 m depth in hard rocks of the Scandinavian Shield using the empirical rock mass characterizations methods of  $Q$  and  $RMR$ . They found that the deformation modulus ranged from 28 to 56 GPa over the 100-m depth range with a mean of 42 GPa and a Standard Deviation 8.9 GPa. The predicted  $k$  using Eq. (3) for these modulus values are also shown on Fig. 11. Note that despite the range in modulus values the measured  $k$  values far-exceed the predictions using Eq. (3). Hence, while Eq. (3) is a reasonable starting point for estimating  $k$  it does not predict the variability that is encountered when stresses are actually measured and highlights the difficulty with estimating horizontal stress magnitudes.

#### 4. Tunnel stability and stress path

Instability for practical engineering purposes is usually assessed by considering a ratio of stress (Demand) to strength (Capacity), i.e., instability is anticipated when the demand exceeds the capacity. Two forms of instability are readily observed around underground openings (Fig. 12): (1) structurally controlled gravity-driven processes leading to wedge type falls-of-ground; and (2) stress-induced failure or yielding.

Structurally controlled falls-of-ground are common in low confining-stress environments at shallow depths or when geometric factors, e.g., at tunnel intersections, reduce the natural confinement. In these situations, wedge-type blocks, driven by gravity loading conditions, are able to fall or slide from the roofs and sidewalls of tunnels. The shear strength ( $\tau$ ) of the discontinuities bounding the blocks or wedges on which separation or sliding takes place can be expressed as

$$\tau = c + \sigma_n \tan \phi, \quad (4)$$

where  $c$  is the cohesion,  $\sigma_n$  is the normal stress acting on the failure plane and  $\phi$  is angle of friction. From Eq. (4),

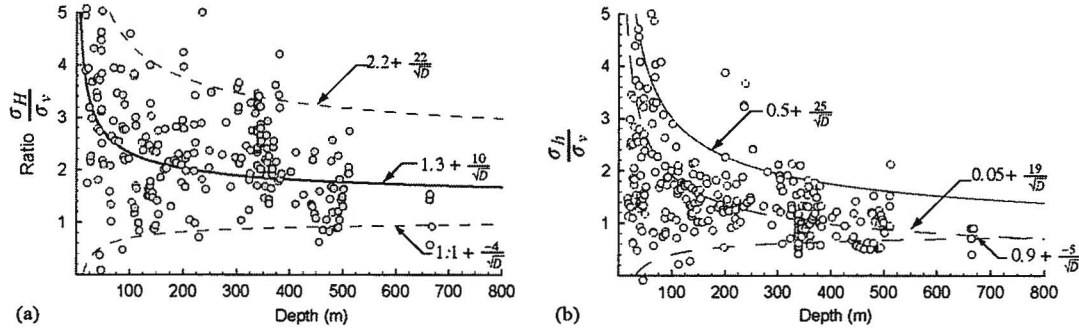


Fig. 10. Horizontal to vertical stress ratios determined from the Scandinavian stress database. (a) Ratio  $\sigma_{Hmax}/\sigma_{vert}$ . (b) Ratio  $\sigma_h/\sigma_{vert}$ .

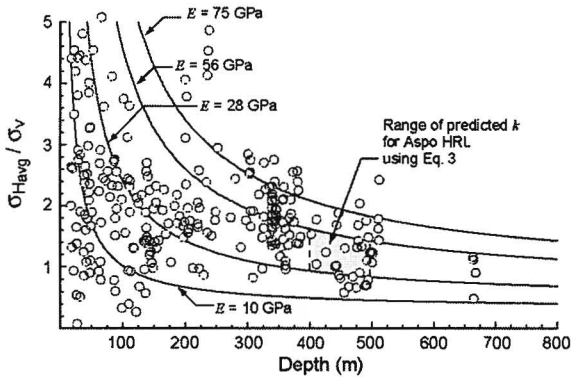


Fig. 11. Relationship between horizontal deformation modulus ( $E$ ) and the ratio of the average horizontal stress to vertical stress, using Eq. (3). Also shown is the measured average horizontal stress to vertical stress ratio for the Scandinavian shield.

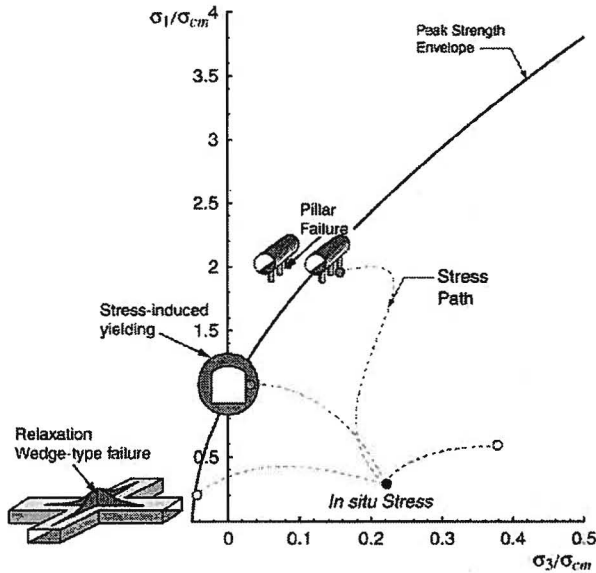


Fig. 12. Generalized stress path that can lead to different modes of instability around underground openings. Note that there are basically two stress paths: (1) loading and (2) unloading. In fractured rock masses the tensile strength is low or nonexistent hence, the unloading path does not have to reach the tensile conditions illustrated above for wedge-type failures to occur.

it can be seen that the strength of these potential wedges is influenced by the confining stress, expressed as  $\sigma_n$ . Despite the importance of confining stress on strength, simple limit-equilibrium wedge analysis do not normally consider the effect of the in situ stresses on this mode of failure [13,14]. While attempts have been made to calculate the effect of confining stress on the self-supporting capacity of the rock or to add a driving force on the demand side of the equation, stress paths (Fig. 12) leading to loss of confinement (e.g., due to geometric factors at intersections) or due to nearby mining (e.g., near a large cavern or in the influence zone of stopes [15]) are seldom considered.

When stress magnitudes reach the rock mass strength, i.e., stress-induced yielding, the designer is faced with deciding the hazard the yielding will create. In weak and soft rocks the yielding may result in large convergence displacements where these displacements are a function of the size of the plastic zone relative to the tunnel diameter. In hard and strong rocks the yielding may result in relatively small convergence displacements as long as the depth of failure is limited and the bulking process in the failing rock is well controlled [16]. In deep-seated failure, large rock mass dilation, e.g., due to geometric incompatibility between blocks of failed rock, may also lead to large deformations due to bulking (volume increase). Furthermore, the yield process in hard rock may occur in a violent manner with the sudden release of stored strain energy. This process is often referred to as violent spalling or strain bursting. Knowing the likely failure process can aid the designer in choosing an appropriate strategy for support design and the excavation sequencing.

Key to determining which failure process is likely to occur is estimating the stress level and the rock mass strength and, in some situations, the rock mass stiffness.

#### 4.1. Role of stress change

When a large excavation, a cavern or a stope, is excavated in the vicinity of an existing tunnel the stress magnitudes near the tunnel wall are altered. Such stress changes were monitored by Kaiser et al. [15] both in the

relaxation zone (in the hanging wall) and in the compression zone (in the back) during the excavation of a panel-shaped stope excavated in high-horizontal stresses. The initial stress state and the recorded change in principal stress are summarized in Table 4. It is important to note that the stress tensor rotates during the excavation of underground opening and that the final principal stresses do not align with the initial principal stresses as illustrated by the measurements by Kaiser et al. [15] and Eberhardt [17].

For a circular excavation the maximum stress level  $SL$  can be found from the Kirsch equations and expressed as

$$SL = \frac{\sigma_{max}}{\sigma_{ci}} = \frac{3(\sigma_1 \pm \Delta\sigma_1) - (\sigma_3 \pm \Delta\sigma_3)}{\sigma_{ci}} \quad (5)$$

The minimum stress level can be expressed in a similar manner and changes accordingly. The linearized, schematic stress path, connecting the initial and the final stress state at the maximum (A) and minimum (B) stress concentration points, for a circular tunnel at an initial stress state of  $\sigma_1^o = 0.24\sigma_{ci}$  and  $\sigma_3^o = 0.24\sigma_{ci}$ , respectively, is presented in Fig. 13. Typically, the minor principal stress decreases near large excavations while the major principal stress may increase or decrease as illustrated by Fig. 12. The minimum and maximum stress levels for a tunnel in the virgin stress field are 0.36 and 0.52, respectively. Mining-induced stress changes, in general, aggravate the stress level. This is illustrated for an assumed increase in the major principal stress  $\Delta\sigma_1$  from 0.24 to  $0.4\sigma_{ci}$ . This change in stress leads to a drastic increase in the maximum  $SL$  from 0.52 at A to 1.0 at A', and a corresponding decrease in the minimum  $SL$  from 0.36 to 0.2. The minimum and maximum stress levels for the two measurement locations are also listed in Table 4.

For the example presented in Table 4, the initial, maximum stress level ( $SL$ ) changes from 0.6 to 1.48 in a highly stressed area and to 0.4 in an area experiencing stress relaxation. As will be discussed later, this will bring a marginally stable excavation, before mining, to deep-seated failure by squeezing, heavy spalling or stress-driven wedge instability at Location 1. The minimum stress level changes from an initially confined

Table 4  
Observed stress level changes at two location near an advancing stope [15]

	Initial stress (MPa)	Stress change location 1	Stress change location 2
$\sigma_1$ or $\Delta\sigma_1$	35.5	45.5	-15.5
$\sigma_2$ or $\Delta\sigma_2$	26	16	-6
$\sigma_3$ or $\Delta\sigma_3$	15.5	5.5	-15.5
Max. $SL$	0.6	1.48	0.4
Min. $SL$	0.07	-0.12	-0.13

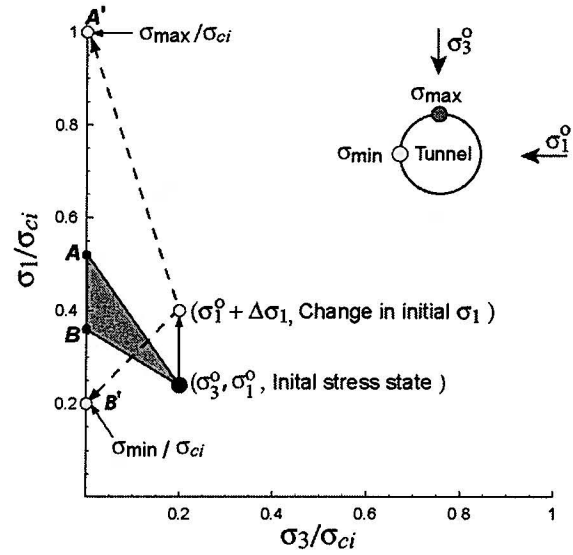


Fig. 13. Schematic stress path for excavation affected by a mining-induced stress change ( $\Delta\sigma_1$ ).

state to a relaxed state at both locations, potentially promoting structurally controlled failure process (see later), particularly when the minimum stress level occurs in the roof of an excavation. Consequently, mining-induced stress path often dominates the behaviour mode of an excavation (Fig. 12).

#### 4.2. Rock mass characterization

Once the stress level has been determined, empirical methods are often used to determine the rock mass characteristics. The Geological Strength Index ( $GSI$ ) was introduced by Hoek et al. [18] and later modified by Hoek and Marinos [19] as a means of estimating the rock mass strength and deformation characteristics. As part of  $GSI$  Hoek et al. [20] suggested that the rock mass deformation modulus ( $E_m$ ) could be estimated by

$$E_m(\text{GPa}) = \left(1 - \frac{D}{2}\right) \sqrt{\frac{\sigma_{ci}}{100}} \times 10^{(GSI-10)/40}, \quad (6)$$

where  $D$  is a factor related to blasting-induced damage that ranges from 0 for no damage to 1 for highly damage rock mass,  $\sigma_{ci}$  is the laboratory uniaxial compressive strength in MPa and  $GSI$  is the Geological Strength Index ranging from 1 for very weak rocks to 100 for massive rocks. Hoek et al. [20] suggested that Eq. (6) is applicable for  $\sigma_{ci} < 100$  MPa, otherwise the square root term is set to unity.

Eq. (6) was established from near surface measurements (plate load tests, etc.). Hence, the corresponding modulus is representative of conditions near excavation walls or for rock masses at shallow depth (< 100 m). At greater depth, particularly in massive to moderately

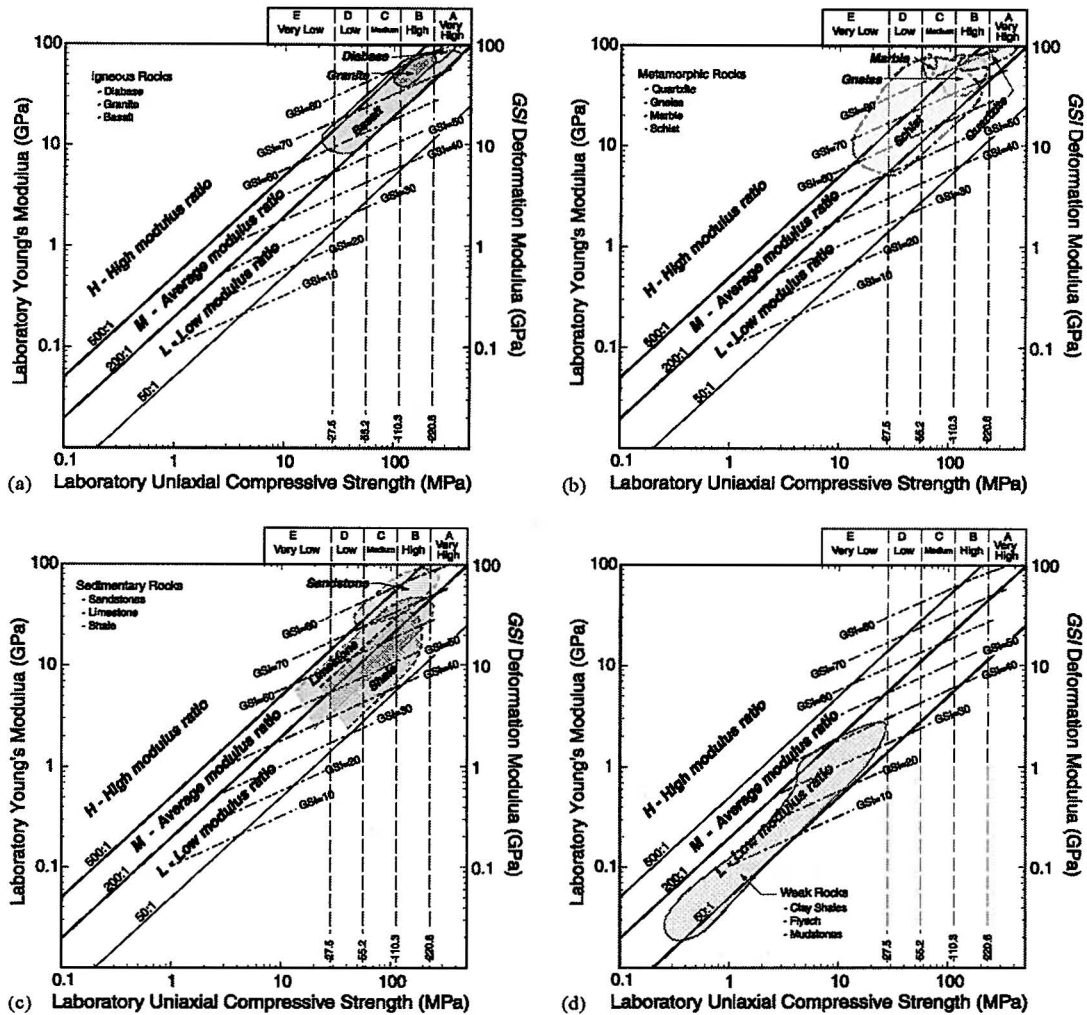


Fig. 14. Relationships between Deere's classification for  $\sigma_{ci}$ , laboratory Young's modulus and geology. Superimposed on the plots is the relationship between rock mass deformation modulus and  $GSI$ . (a) Igneous rocks. (b) Metamorphic rocks. (c) Sedimentary rocks. (d) Weak rocks.

jointed rock, Eq. (6) may underestimate the rock mass modulus of the virgin rock mass.

Using Eq. (6) it is possible to establish relationships with  $E_m$ ,  $\sigma_{ci}$  and  $GSI$ . Fig. 14 shows these relationships for  $GSI$  ranging from 10 to 80 in increments of 10. For  $GSI > 90$  equation gives unrealistically high deformation modulus values. Also superimposed on these relationships is the rock classification system introduced by Deere [21].

Deere's classification relates  $\sigma_{ci}$  and laboratory Young's modulus grouped according to geology, i.e., Igneous, Metamorphic and Sedimentary rocks. Fig. 14d includes additional data for weak rocks such as Clay shales, Mudstones and Flysch. From Deere's classification the relationship between  $\sigma_{ci}$  and Young's modulus tends to follow the trend lines in Fig. 14 given by high, average and low modulus ratios.

Because  $E_m$  cannot be greater than the Laboratory Young's modulus, it is reasonable to present both

classifications on Fig. 14. It can be seen from Fig. 14 that for certain rock types there are practical limits for  $GSI$  and in Fig. 14 these represent the maximum values for  $GSI$  given by Hoek et al. [20] guidelines. Of course, the actual  $GSI$  for a the rock mass may be lower than those given, depending on the intensity of fracturing. For example, for weak rocks  $GSI$  has the largest range 0–50, but it is not practical to have  $GSI$  values greater than 50.  $GSI$  greater than 50 would violate the relationships established by Deere. Likewise for hard rocks, i.e., for granites, the maximum  $GSI$  values would be expected to range from 70 to 80. This implies that Fig. 14 can be used to establish the maximum likely range of  $GSI$  and the corresponding rock mass deformation modulus. The range of  $GSI$  values and the corresponding deformation modulus values for the various rock types are used in the following section to establish the likely behavioural mode of failure described at the beginning of this section:

(1) stress-induced large-scale deformations, or (2) stress-induced spalling.

#### 4.3. Stress controlled instability

Because in situ stress drives failure processes, the most common way of utilizing stress data in design is to determine the stress level as a ratio of the in situ stress state to the strength of the rock mass, or *visa versa*. This ratio is frequently used as an index to assess the risk of over stressing the rock mass for the design of underground openings. For example, Muirwood [22] and Adyan et al. [23] use the ratio of the laboratory uniaxial compressive strength  $\sigma_{ci}$  to the overburden stress  $\sigma_v$  to identify squeezing conditions in weak rocks. They concluded, based on civil engineering tunnelling case histories <400 m depth, that squeezing conditions were encountered when  $\sigma_{ci}/\sigma_v > 2$ .

Hoek and Brown [13] examined square tunnels in deep South Africa gold mines and introduced a stress to strength ratio ( $\sigma_1/\sigma_{ci}$ ) as an index for tunnel stability in hard brittle rocks. Their stability index ranges from 0.1 through 0.5 and can be briefly described as follows: the rock mass response was elastic if  $\sigma_1/\sigma_{ci} < 0.15$ , minor to moderate instability occurred if  $\sigma_1/\sigma_{ci}$  falls between 0.15 and 0.35, and severe instability encountered when  $\sigma_1/\sigma_{ci} > 0.4$ , i.e., heavy support required to stabilize the opening. In these approaches, the stress level is typically defined in terms of the overburden stress  $\sigma_v$  or  $\sigma_1$  the major far-field in situ principal stress.

Fig. 15a illustrates these two modes of failure and the possible outcome. In order to make the risk/hazard assessment in Fig. 15a the designer must know the strength of the rock mass and the in situ stress state. More importantly the designer also needs information that will indicate the likely behaviour.

##### 4.3.1. Instability in weak and soft rocks

In establishing the strength to stress ratio discussed above, the use of a single value to represent the stress tensor may be questioned. The theoretical basis for this argument is that weak rocks are not capable of sustaining a shear stress over geological time and tend to fail until the in situ stresses are equalized. There is also evidence, based on back analysis of tunnel deformations in very weak flysch in Greece, that the in situ stresses tend to be isotropic in these rocks (Hoek, pers. comm.). Hence, in weak rocks an index that utilizes only the maximum stress appears appropriate.

Based on field observations and measurements Sakurai [24] first suggested that tunnel strains for weak rocks, expressed as tunnel convergence normalized to the tunnel diameter, in excess of 1% are associated with the onset of tunnel instability. Field observations by Chern et al. [25] also supported Sakurai's proposed strain limit. Recent work by Hoek [26] using the Hoek–

Brown failure criterion and the Geological Strength Index showed that for weak rocks  $GSI < 30$ , the depth of the plastic yield zone around a tunnel subjected to more or less uniform in situ stress increased significantly when the ratio of the rock mass strength ( $\sigma_{cm}$  determined from  $GSI$ ) to the average far-field in situ stress was less than 0.25 (Fig. 15b).

Hoek [26] noted that for very weak rocks the diameter of the plastic yield zone around a tunnel at depth could approach 5 times the diameter of the tunnel. For large yield zones, the tunnel designer is concerned about controlling the associated radial displacements. Hoek [27] provided guidelines for the support in weak rocks based on tunnel strain (convergence normalized to the tunnel diameter) and noted that when tunnel strain is less than 1% support problems are unlikely (Fig. 15d). For such situations the ratio of rock mass strength to the far-field in situ stress was greater than 0.35. For  $\sigma_{cm}/\sigma_1 < 0.1$ , severe squeezing conditions with more than 5% strain are to be anticipated.

##### 4.3.2. Instability in brittle hard rocks

In hard rocks, in situ stresses tend to be anisotropic (see Section 3). Thus the tangential stresses on the boundary of the excavation are not uniform but concentrated locally and hence these induced stresses are not just dependent on the magnitude of the major principal stress, as is the case in weak rocks. Therefore, it is meaningful to introduce a measure of stress concentration when assess instability in hard rocks. Martin et al. [28] used the maximum tangential stress ( $\sigma_{max} = 3\sigma_1 - \sigma_3$ ) for a circular opening as an indicator of this stress concentration, where  $\sigma_1$  and  $\sigma_3$  are the far-field in situ stress. Because  $\sigma_{max}$  depends on both principal stresses, it can also be expressed in terms of stress ratio  $k = \sigma_1/\sigma_3$  as

$$\sigma_{max} = (3k - 1)\sigma_3. \quad (7)$$

Around underground openings, at depth, in brittle hard rocks the commonly observed mode of instability is spalling. Spalling is the process of new stress-induced fractures growing parallel to the excavation boundary producing thin “slabs” of rock. This fracturing is generally referred to as brittle failure. Initially, at intermediate depths, these failure regions are localized near the tunnel perimeter but at great depth the fracturing may envelope the whole boundary of the excavation. Martin et al. [28] documented tunnel spalling case histories and demonstrated that the depth of spalling ( $d_t/a$ ) was linear with increasing stress to strength ratio expressed as the maximum tangential stress ( $\sigma_{max}$ ) on the boundary of the opening normalized to the laboratory uniaxial strength. Their equation is recast here with the laboratory uniaxial strength

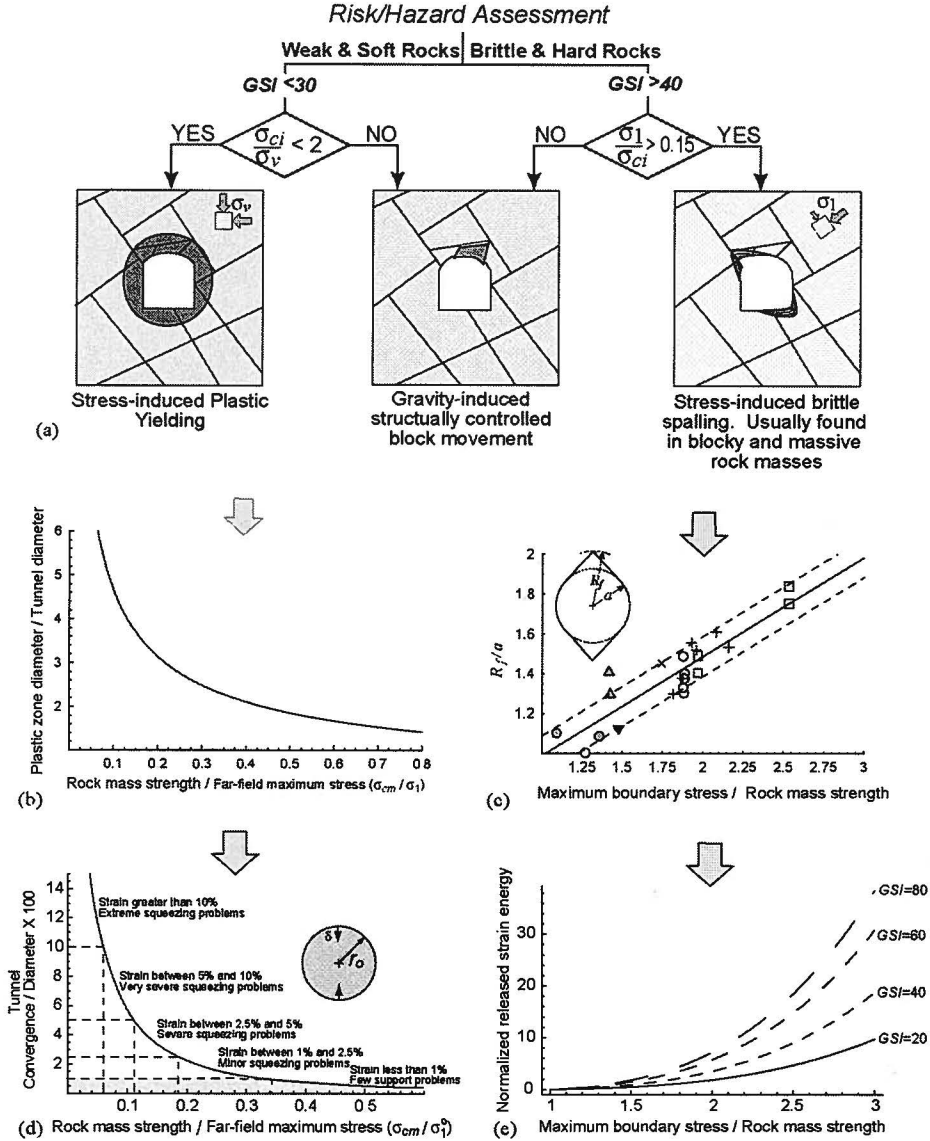


Fig. 15. Illustration of the two common modes of failure and associated hazards observed around under-ground openings. (a) Decision tree. (b) Depth of plastic zone, data from [26]. (c) Depth of spalling, data from [28]. (d) Deformation hazard, data from [27]. (e) Strain energy release hazard.

replaced with the uniaxial rock mass strength ( $\sigma_{cm}$ ) as

$$\frac{d_f}{a} = 0.48 + 0.5 \frac{\sigma_{max}}{\sigma_{cm}} \quad (8)$$

and the results presented in Fig. 15c. The results from Ref. [28] showed that for spalling conditions in hard rocks  $\sigma_{cm} = C\sigma_{ci}$ , where  $C \approx 0.3-0.5$ .

The rock masses in the case histories examined by Martin et al. [28] ranged from Sedimentary siltstones ( $\sigma_{ci} = 36$  MPa) to Igneous granites ( $\sigma_{ci} = 240$  MPa). Despite the range in uniaxial compressive strength and rock mass strength, the stress-induced spalling process resulted in the formation of “v-shaped” notches. The

greatest depth of the “v-shaped” notch reported by Martin et al. [28], at  $\sigma_{max}/\sigma_{cm} = 2.5$ , was slightly less than one tunnel radius.

One of major risks associated with stress-induced spalling in hard rocks is the potential for the violent release of stored strain energy. Aglawe [29] examined this issue and showed that the released strain energy ( $\Delta RE$ ) as an opening extends from a circle to an ellipse can be expressed as

$$\Delta RE = \frac{\pi p^2}{2E/(1-\nu^2)} ((ab + 2a^2 - 3a^2) + (2b^2 + ab - 3a^2)k^2 - (2ab - 2a^2)k), \quad (9)$$

where  $a$  and  $b$  are the axis of the ellipse,  $p$  is far-field stress,  $k$  is the stress ratio, and  $E$  is Young's modulus and  $\nu$  is Poisson's ratio. For this energy release calculation, it is assumed that the rock in the entire zone described by the depth of failure fails at once. If the failure process proceeds by sequential violent slabbing, the released energy is smaller. Using  $GSI$  to determine Young's modulus (Eq. (6)), and the linear relationship for the depth of failure in Eqs. (8), (9) was used to calculate the change in the released strain energy for increasing values of  $GSI$  Fig. 15e. As expected, as the quality of the rock mass improves, the amount of strain energy released increases. However, note that for relatively small spalling depths, the increasing rock mass quality only slightly increases the amount of energy released.

#### 4.4. Summary

The analysis of underground openings requires knowledge of basically two variables: (1) in situ stress, and (2) rock mass strength. Once these variables are defined the designer must then select the most appropriate design process depending on the anticipated failure process. Fig. 15 outlines a generalized flow chart for this with focus on determining whether the hazard stems from large displacements due to plastic yielding or from spalling failure, possibly with strain energy release.

Regardless of the hazard, in situ stress plays a key role in the design process. Issues associated with this design process are discussed in the following sections.

### 5. Assessment of instability in the design process of tunnels in hard rocks

In the previous section it was demonstrated that while general trends can be used to estimate the likely stress magnitudes, stress variability beyond those estimates must be anticipated. In this section, the impact of in situ stress on the stability of underground openings is illustrated. Examples are also provided illustrating how stress variability can be incorporated into the design of underground openings in hard rocks.

#### 5.1. Shallow tunnels and high horizontal stresses

It was shown in Section 3.2 that the horizontal stress magnitudes can exceed the weight of the overburden at relatively shallow depths (see Fig. 9). These high horizontal stresses can be an advantage when constructing shallow tunnels and caverns. For example in 1991 the Olympic Ice Hockey Cavern was successfully constructed at Gjøvik, Norway with a rock cover of only 25–50 m [30]. Permanent rock reinforcement for this 62-m span cavern consisted of only 100 mm

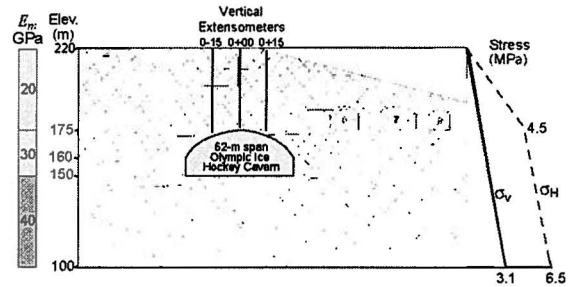


Fig. 16. General layout for the 62-m span Olympic Ice Hockey Cavern at Gjøvik, Norway. Also shown are the high horizontal stresses, the rock mass modulus  $E_m$  and the joint patterns, modified from Ref. [30].

steel-fibre reinforced shotcrete and systematic bolting and cablebolting in alternating 2.5 and 5.0 m centre-to-centre patterns. The successful construction of this large cavern was attributed in part to high horizontal stresses [30].

The general geologic conditions for the Olympic Ice Hockey Cavern are summarized in Fig. 16. The Precambrian gneissic rock mass had a mean  $Q$  value of 9.4 with three distinct zones of rock mass moduli ( $E_m$ ) determined from drill core and seismic tomography. Two distinct joint patterns were mapped and core logs gave an average  $RQD$  value of 67%. The joints were generally irregular, rough walled and with quite large variations in dip and strike. The joint pattern in Fig. 16 and the distinct element program  $UDEC$  was used by Barton et al. [30] to model the cavern behaviour during construction.

In situ stress measurements for the Olympic Ice Hockey Cavern indicated the high horizontal stresses shown in Fig. 16. A stress analysis was carried out using the finite element program Phase2<sup>3</sup> for the in situ stress and rock mass modulus conditions given in Fig. 16. Fig. 17 shows the continuum stress trajectories around the hockey cavern upon completion of the excavation. The stress concentration in the roof of the cavern tend to compress the rough joints shown in Fig. 16. If the maximum stress had been vertical, instead of horizontal, such compressive stresses in the cavern roof would not exist.

The construction of the hockey cavern was monitored with vertical extensometers installed from the ground surface (Fig. 16). The results from three extensometers installed near the centre of the cavern are reproduced in Fig. 18. Barton et al. [30], using the distinct element program  $UDEC$ , predicted the displacements at the crown of the tunnel to be 4.3 mm. In their model they used the rock mass moduli values and joint distributions in Fig. 16. To predict the displacements using a continuum model such as Phase2 an equivalent rock mass modulus needs to be established. At presents the

<sup>3</sup> Available from [www.rocsience.com](http://www.rocsience.com)

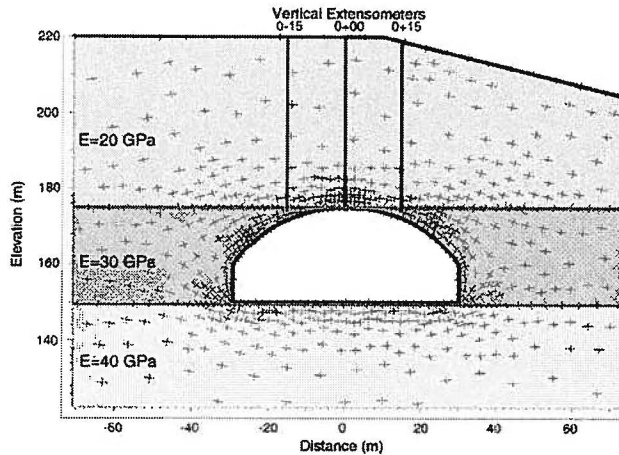


Fig. 17. Stress trajectories around the Olympic Ice Hockey Cavern at Gjøvik, Norway upon completion of the excavation using the continuum model in Phase2.

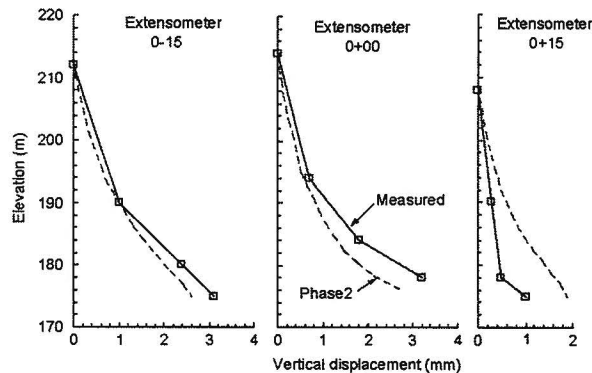


Fig. 18. Extensometer results from the Olympic Ice Hockey Cavern at Gjøvik, Norway compared to Phase2 results with a rock mass modulus of 5 GPa. The extensometer results were taken from Ref. [30].

rock mass modulus is determined using equations such as those shown in Fig. 19 relating modulus to rock mass quality. Accordingly, the rock mass moduli as shown in Fig. 16 corresponds to rock mass quality ranging from  $Q = 4-20$  or  $RMR = 60-70$ . If these rock mass moduli in Fig. 16 are used, the maximum predicted displacement is less than 1 mm. However, if the continuum rock mass modulus is reduced to 5 GPa, to take into account nonlinear effects of joint closure and shear, the Phase2 results are in better agreement with measured results (Fig. 18). Clearly this modulus is significantly lower than anticipated based on the data shown in Fig. 19 and the corresponding equations representing this data. No attempt was made to refine the modulus value beyond 5 GPa as the purpose was to illustrate the difficulty in choosing the representative rock mass modulus. Further research is needed in this area.

Note that despite the size of the cavern the maximum displacements measured by the extensometers is less

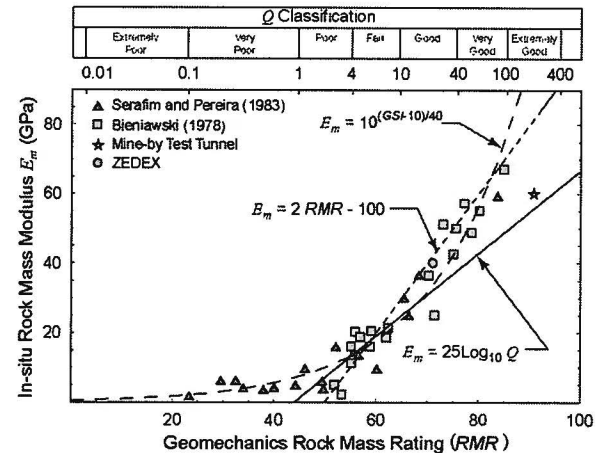


Fig. 19. Compilation of the correlations of rock mass modulus  $E_m$  and rock mass quality. Data compiled from Refs. [43,44].

than 4 mm and that the displacements at Ext. 0 + 15 are less than half those measured by the other two extensometers. The reason for the reduction in vertical displacement at Ext. 0 + 15 is due to the sloping ground shown in Fig. 16 in combination with the high horizontal stress.

While continuum models can be used to gain insight into deformation patterns care must be used in establishing the input parameters, particularly the rock mass modulus. Empirical rock mass classification systems, such as those shown in Fig. 19, are useful for establishing likely modulus values as long as the loading conditions are comparable. However, as demonstrated here choosing a continuum modulus to represent a discontinuum is not straight forward and should be based on applicable tests following representative stress paths. Nonetheless, the positive impact of the horizontal stresses on design of shallow caverns is demonstrated by both continuum and discontinuum models.

Since the construction of the Olympic Ice Hockey Cavern at Gjøvik, Norway, two major tunnelling projects in Stockholm, Sweden have also benefited from high horizontal stresses. Both the rapid train link from Arlanda international airport to central Stockholm and the public traffic road tunnel system south of Stockholm included large span (up to 15 m) tunnels at relatively shallow depths. For these tunnels the depth of rock cover ranged from a few meters to approximately 50 m. Local construction experience suggests that the safe excavation of these large span tunnels is in part due to the confinement provided by the high horizontal stresses experienced at shallow depth in the Scandinavian shield.

## 5.2. Loss of confinement and gravity induced instability

One of the more common problems found in deep Canadian mines that use bulk mining methods is

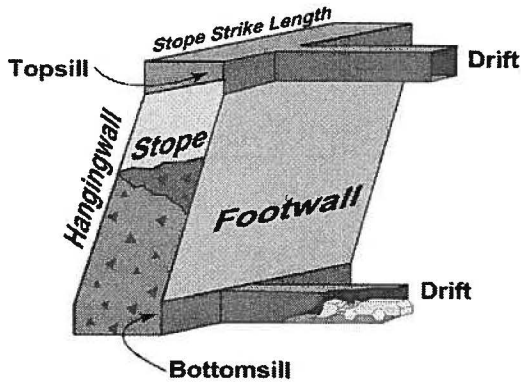


Fig. 20. Illustration of typical bulk-mining stope.

instability of the hanging wall (Fig. 20). This problem prompted the development of the empirically derived Stability Graph method for stope design [31,32]. The stope stability graph, while often adequate for estimating the dimensions of stopes, does not estimate the amount of raveling the hanging wall may experience (causing dilution) or does not properly consider the effects of stress path in the surrounding rock mass (Fig. 12). In bulk mining, stope heights typically range from 20 to 125 m, with the stope strike-length constrained by the stability of the hanging wall (Fig. 20). The width of these stopes varies depending on the particular mining method and the width of the orebody, but invariably the excavation of such rectangular-shaped openings leads to the formation of low confining stresses ( $\sigma_3$ ) or in many cases, tensile stresses in the hanging wall. This notion in combination with the low tensile strength of a fractured rock mass was used by Alcott et al. [33], Martin et al. [34] and Martin et al. [35] to evaluate hanging wall instability risks in hard rock mines. In a detailed investigation of the effects of stress relaxation on excavation stability Diederichs and Kaiser [36] have shown that relaxation, causing near zero stress conditions tangential to excavation spans, drastically reduce the self-supporting capacity of fractured ground surrounding an excavation. In addition, this relaxation can also drastically reduce the effectiveness of frictional support systems, such as plain-strand cablebolts, which are often used to support hanging walls [37]. The effect of mining-induced stress changes on excavation stability and support performance have also been discussed by Kaiser et al. [15] on the Winston Lake case study. In the following, the effects of confinement loss are illustrated using a mining case history from the Canadian Shield.

Martin et al. [35] presented detailed analyses of raveling of the hanging wall at a hard rock mine in Sudbury, Canada. Only a brief summary of their findings is presented here. The massive sulphide ore zone at depth was 300 m along strike and 45 m in width from footwall to hanging wall and dipped between 65° to 85°. A general three-dimensional view of the mine

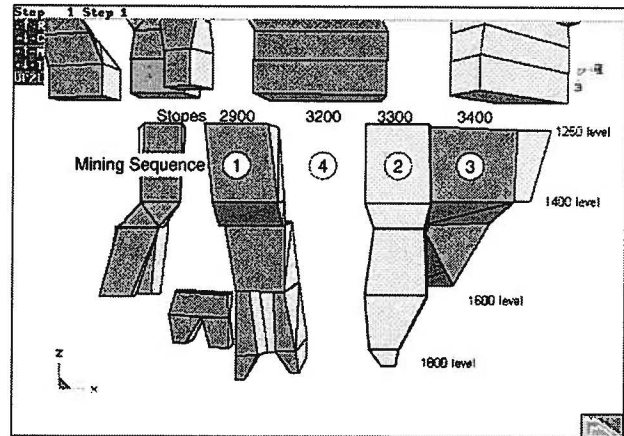


Fig. 21. General view between 1250 Level and 1800 Level looking towards mine north.

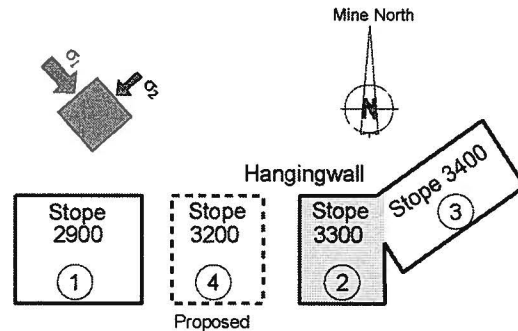


Fig. 22. Plan view of open stopes and stoping sequence (circled numbers). Stope 3300 was stable until mining of 3400 stope commenced.

from the 1250 Level to the 1800 Level is shown in Fig. 21 and a plan view of the 1250 mining Level is shown in Fig. 22. The mining sequence proposed for this mining block is also shown in Fig. 22. Mining of stopes 2900 and 3300 was carried out without incident, with stope 3300 remaining open and stable for approximately 1 year. The mining of stope 3400 was coincident with the raveling of the 3300 hanging wall.

The transverse stopes averaged 35 m in width, 45 m in length and over 180 m in height. Experience at the mine indicated stopes of these dimensions were stable. However 3300 stope, which had similar good quality rock mass conditions, experienced significant hanging wall problems. The hanging wall rock mass consisted of blocky norites with one subvertical joint set at approximately 1 m spacing and a second set of horizontal continuous joints also at approximately 1 m spacing. These fracture sets formed potential wedges in the hanging wall and backs of stopes. However, simple wedges do not usually lead to progressive raveling, particularly when the Geological Strength Index ranges from 60 to 85. The corresponding Hoek–Brown

Table 5  
GSI and Hoek–Brown strength parameters

	GSI	
	60	85
$\sigma_{ci}$ (MPa)	230	230
$m_i$	28	28
$m_b$	6.71	16.39
$s$	0.012	0.189
$E_m$ (GPa)	27	80
$\sigma_{cm}$ (MPa)	25	100
$\sigma_{tm}$ (MPa)	−0.40	−2.65

parameters for these strength conditions are given in Table 5. Note that the rock mass tensile strength ranges from −0.4 to −2.65 MPa.

The 3300 stope, although stable for approximately 1 year upon completion, experienced extensive hanging wall ravelling after the mining of 3400 stope commenced. Three-dimensional elastic numerical analyses of the mining sequence leading up to the hanging wall instability was carried out using MAP3D<sup>4</sup> with the mine-wide geometry shown in Fig. 21. The MAP3D results from those analyses are summarized in Fig. 23 in the form of  $\sigma_1$ ,  $\sigma_2$  and  $\sigma_3$  contours. Fig. 23 shows that because of the stope geometry, a zone of relaxation, extends several tens of metres into the hanging wall of the 3300 stope after 3400 stope was excavated. The MAP3D results indicate that in the caved region (confirmed by cavity surveys) the minimum principal stress ( $\sigma_3$ ) ranges from approximately 0 to −1 MPa, the intermediate principal stress ( $\sigma_2$ ) from 0 to approximately 20 MPa, and the maximum principal stress ( $\sigma_1$ ) from 5 to 25 MPa. However, it is only the  $\sigma_3$  contours that have the same general shape as the profile from the cavity survey (Fig. 23c). It should be noted that the MAP3D model does not contain the development drifts. The inclusion of these additional tunnels in the numerical model would likely improve the agreement with the cavity survey and the  $\sigma_3$  contours near the top and bottom of the stope.

A series of 12 evenly spaced stress grid lines in MAP3D were used to determine the elastic stress state over the hanging wall of stope 3300. The calculated stress states near the excavation wall are given in Fig. 23d, where the open squares represent the stress state at points where failure occurred, as determined from the cavity survey. The open triangles represent locations in a stable stress state. It is evident from Fig. 23d that failure or ravelling occurs when the confining stress is less than zero. Given that the tensile strength of the rock mass ranges from approximately −0.40 to −2.65 MPa,  $\sigma_3 > 0$  MPa would be sufficient to prevent tensile failure. The notion that a simple

confining stress (tensile strength) criterion can be used to assess hanging wall stability and dilution potential has also been reported by Martin et al. [34] and Alcott et al. [33].

The shape and extent of the  $\sigma_3 = 0$  isosurface in the hanging wall of 3300 stope was determined using the three-dimensional boundary element program Examine3D<sup>5</sup> (Fig. 24). The location of the isosurface is generally in good agreement with the results from the cavity survey and field observations. More importantly the analysis showed that without the mining of 3400 stope, the 3300 stope was stable, emphasizing the importance of sequencing to control the extent of rock relaxation when assessing the stability of mine openings.

### 5.3. Assessing the spalling potential: a risk-based approach

In Fig. 15 a procedure was outlined for assessing the potential for spalling. In summary spalling occurs when the maximum tangential stress ( $\sigma_{max}$ ) on the boundary of an underground opening exceeds the rock mass strength ( $\sigma_{cm}$ ) expressed as

$$\sigma_{max} \geq \sigma_{cm}. \quad (10)$$

As noted by Martin et al. [28], the rock mass strength can be expressed in terms of the uniaxial laboratory strength ( $\sigma_{ci}$ ):

$$\sigma_{cm} = C\sigma_{ci}, \quad (11)$$

$C$  is a constant derived from laboratory tests and/or back analysis. For situations, where the minor principal stress is equal to the overburden stress, the Factor of Safety against spalling around a circular opening can then be expressed as

$$\text{Factor of Safety} = \frac{C\sigma_{ci}}{\gamma D(3k-1)}, \quad (12)$$

where  $\gamma$  is the unit weight of the rock mass,  $D$  is the depth and  $k$  is the stress ratio. To utilize a risk-based approach to assess the spalling potential the input(s) for Eq. (12) must be expressed as probability distributions.

The distribution of the uniaxial compressive strength is often assumed to be normally distributed. Tests (83) results on relatively homogeneous Lac du Bonnet granite carried out over a 15 year period are presented in Fig. 25. The  $COV$  is about 13% for this rather uniform rock. Using @Risk<sup>6</sup> a truncated normal distribution provides a reasonable fit to the data.

@Risk was also used to provide a best-fit distribution for the stress ratio between the depths of 400 and 700 m in Fig. 10a. The Weibull Distribution with a  $COV$  of 70% given in Fig. 26 provided a reasonable fit.

<sup>4</sup> Available from <http://www.map3d.com/>

<sup>5</sup> Available from <http://www.rocscience.com/>

<sup>6</sup> Available from Palisade Corporation <http://www.palisade.com/>

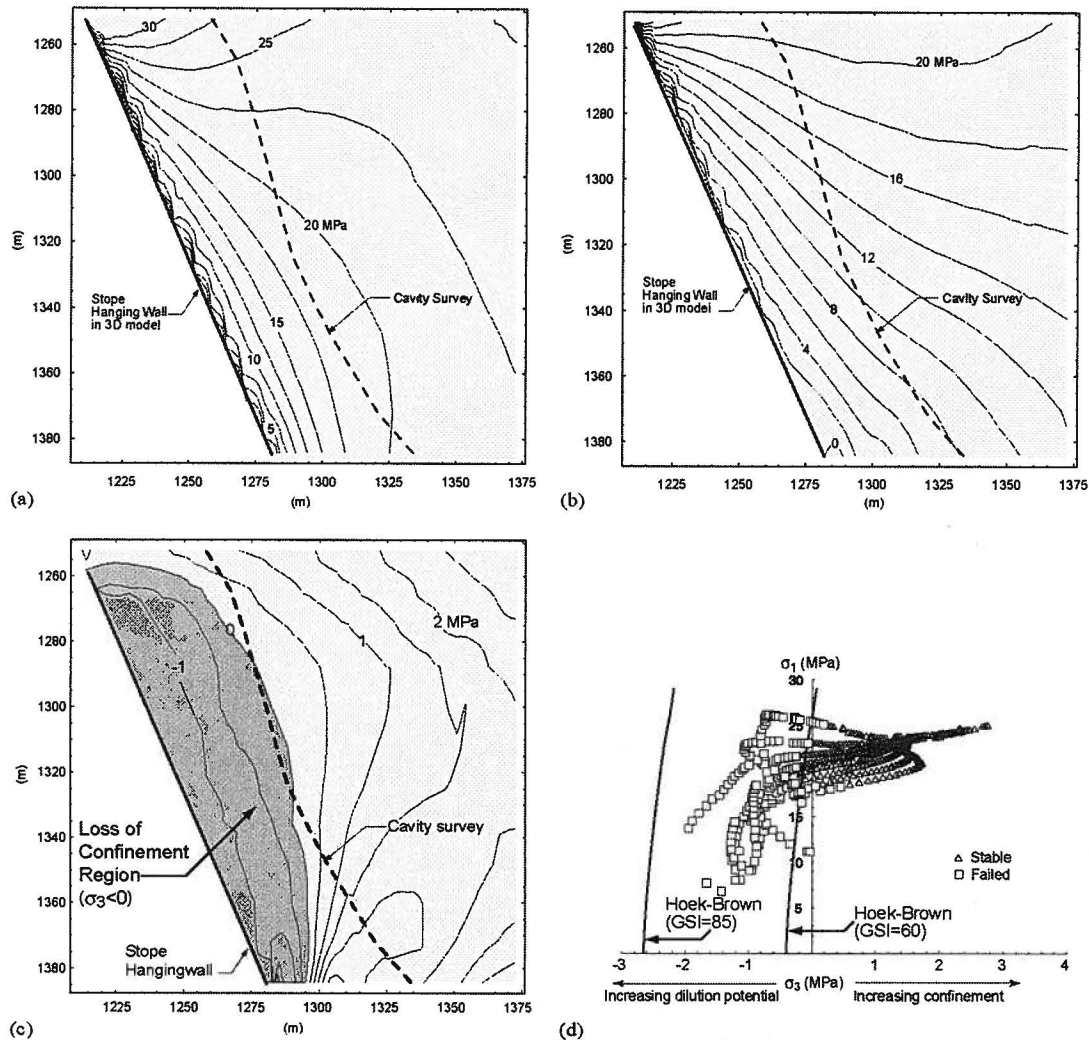


Fig. 23. Vertical section through 3300 Stope looking towards mine west showing the contours for  $\sigma_1$ ,  $\sigma_2$ ,  $\sigma_3$  and the results from the cavity survey. Also shown are the stress paths for the hanging wall obtained using MAP3D. At the Stope wall  $\sigma_2$  is oriented out of the plane in an East-West direction (see Fig. 22). The irregular contours close to the stope wall are related to the numerical sampling points. (a) Sigma 1 contours. (b) Sigma 2 contours. (c) Sigma 3 contours. (d) Stress paths for hangingwall.

Using these distributions for uniaxial strength (Fig. 25), stress ratio  $k$  (Fig. 26), the distribution of the Factor of Safety for spalling was established (Fig. 27). The mean Factor of Safety is 1.18 but there is only a 20% probability that the Factor of Safety will fall below unity. In other words for a 100 m long tunnel there is a potential for 20 m to experience spalling. Obviously this is only true if the rock strength is randomly distributed in space. If strengths are spatially correlated with large-scale geological domains, this needs to be considered in the analysis.

While the example above is relatively simple, it provides a useful means of assessing risk at the early stages of a project when site specific data is in the early stages of data collection.

The Generalised Point Estimate Method, developed by Rosenbleuth (1981) and discussed in detail by Harr

[38], can be used for rapid calculation of the mean and standard deviation of a quantity such as a factor of safety which depends upon random behaviour of input variables. Hoek [39] discussed the application of this technique to the analysis of surface crown pillar stability while Pine [40] has applied this technique to the analysis of slope stability and other mining problems. To calculate a quantity such as a factor of safety, two point estimates are made at one standard deviation ( $\sigma$ ) on either side of the mean ( $\mu \pm \sigma$ ) from each distribution representing a random variable. The factor of safety is calculated for every possible combination of point estimates, producing  $2n$  solutions where  $n$  is the number of random variables involved. The mean and the standard deviation of the factor of safety are then calculated from these  $2n$  solutions.

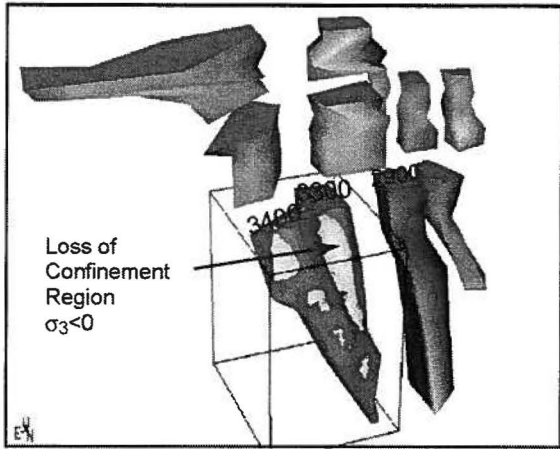


Fig. 24. The  $\sigma_3 = 0$  isosurface obtained from the three-dimensional numerical program Examine3D after mining the 3400 stope.

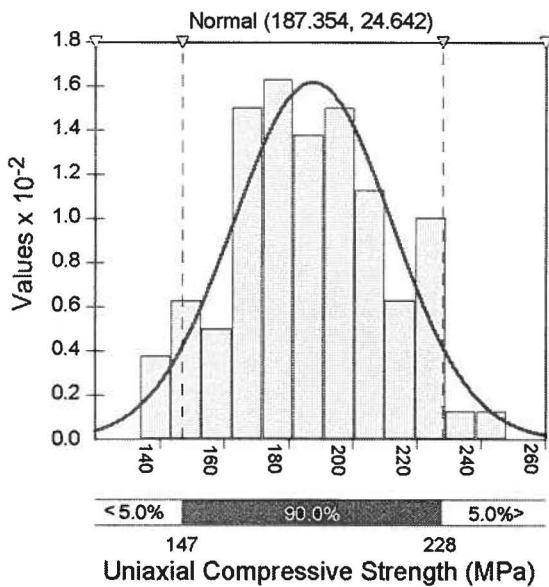


Fig. 25. The Normal Distribution for the laboratory uniaxial compressive strength (UCS) of Lac Du Bonnet Granite.

While this technique does not provide a full distribution of the output variable, as do the Monte Carlo and Latin Hypercube methods, it is very simple to use for problems with relatively few random variables and is useful when general trends are being investigated. When the probability distribution function for the output variable is known, for example, from previous Monte Carlo analyses, the mean and standard deviation values can be used to calculate the complete output distribution.

#### 5.4. Stress variability and depth of failure

In Section 3 it was demonstrated that variability in stress magnitudes must be anticipated. The practical relevance of this variability or uncertainty in the stress

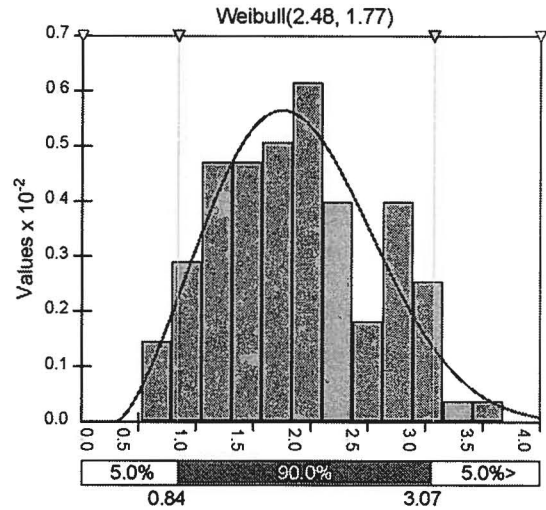


Fig. 26. The Weibull Distribution for the stress ratio  $k$  data given in Fig. 10a.

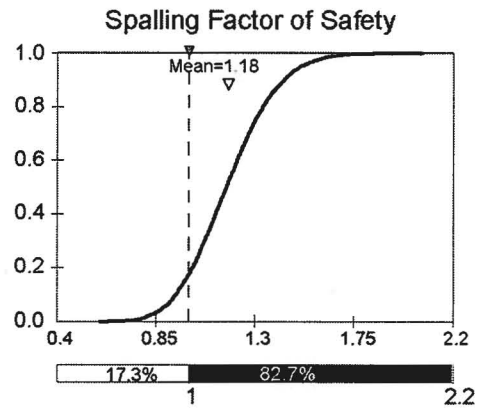


Fig. 27. The distribution of the factor of safety against spalling using the distribution for the uniaxial strength, the stress ratio  $k$  and Eq. (12).

magnitude can best be illustrated using the depth of failure data from AECL's Mine-by Experiment [41]. This 50-m-long circular tunnel was excavated using mechanical rock breakers in relatively homogenous massive granite at the 420 m Level of AECL's Underground Research Laboratory (URL), in Southeastern Manitoba. The URL is located in the Lac du Bonnet batholith of the Canadian Shield. The stress conditions at the URL are given by Martin [42] and the in situ stress state for the Mine-by Experiment are given by Martin et al. [41] in Table 6.

Based on the results of Martin et al. [28] the depth of failure ( $d_f$ ) in hard rocks can be estimated by

$$d_f = a(1.25SL - M), \quad (13)$$

where  $SL$  is given by Eq. (5) and  $M$  is a constant that depends on the rock type and its brittle failure

Table 6  
Summary of the in situ stress tensor determined at the end of the experiment, after [41]

	$\sigma_1$	$\sigma_2$	$\sigma_3$
Magnitudes (MPa)	$60 \pm 3$	$45 \pm 4$	$11 \pm 4$
Trend/plunge (deg)	145/11	054/08	290/77

characteristics. Based on a number of case studies, Martin et al. [28] established  $M = 0.51 \pm 0.05$ .

For the Mine-by Experiment, the following variables and their associated COVs are considered representative of the site conditions:

Vertical stress = 11 MPa,  $COV = 0\%$ ,  
 $k_{max} = 5.45$ ,  $COV = 2\%$ ,  
 $\sigma_{ci} = 224$  MPa,  $COV = 13\%$ .

All variables are assumed to be noncorrelated even though it is expected that  $\sigma_{ci}$  and  $M$  are correlated ( $COV(C) = 0\%$ ). The observed cumulative distribution functions of the depth of failure, presented in Fig. 28, are compared to the predicted distribution functions.

With  $M = 0.51$ , the predicted, average depth of failure is approximately 0.45 m with a  $COV = 28\%$  which gives a depth of failure about 0.1 m greater than the measured depth of failure (Fig. 28a). However, the predicted and measured cumulative distribution functions are significantly different. While the prediction agrees well with the maximum depth of failure (0.8 m), the prediction suggests that only <5% of the tunnel should experience depths of failure of <0.25 m while 35% of the tunnel actually experienced <0.25 m deep failure.

By varying the range for the stress and strength parameters, much better fit can be achieved. For example, by assuming a  $COV(k_{max})$  of 30% and  $M = 0.58$ , excellent agreement between measurements and predictions can be achieved. However, because of the extensive stress measurement campaign for the Mine-by Experiment the variability in depth of failure cannot be attributed to stress variability. Hence, the variability in depth of failure has to be attributed to variability in the strength parameter.

With  $COV(k_{max})$  of 2%,  $M = 0.66$  and a  $COV(\sigma_{ci}) = 32\%$ ,<sup>7</sup> the observed average depth of failure and the cumulative distribution function can be matched (Fig. 28b). In this case the depth of failure is over-estimated with about 10% of the tunnel having a depth of failure > 0.8 m, suggesting that the strength is not symmetrically distributed as assumed for all analysis presented here. Nevertheless, it is evident that the variability in the predicted depth of failure, (for  $M = 0.66$  at an average depth of failure of 0.39 m with a

<sup>7</sup>Typical  $COV$  of  $\sigma_{ci}$  from standard testing programs range from 25% to 30%.

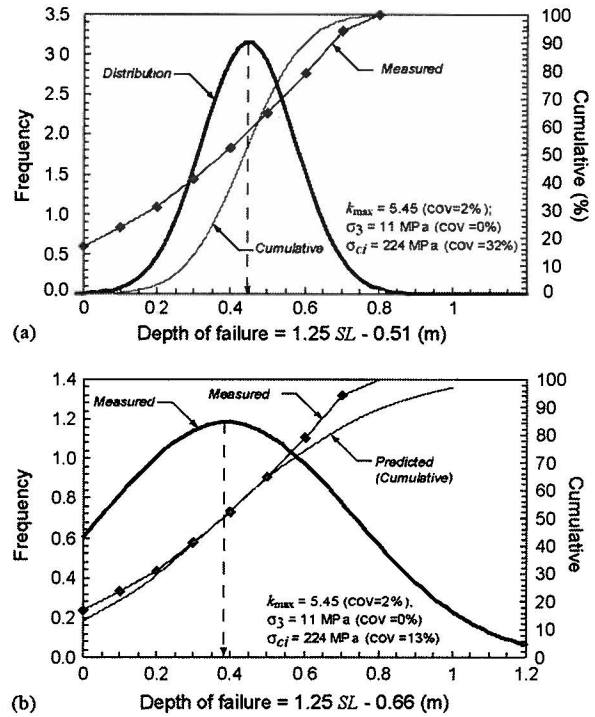


Fig. 28. Predicted probability density and cumulative distribution function for (a)  $M = 0.51$  and (b)  $M = 0.66$  compared with measured depth of failure at AECL's Mine-by Experiment.

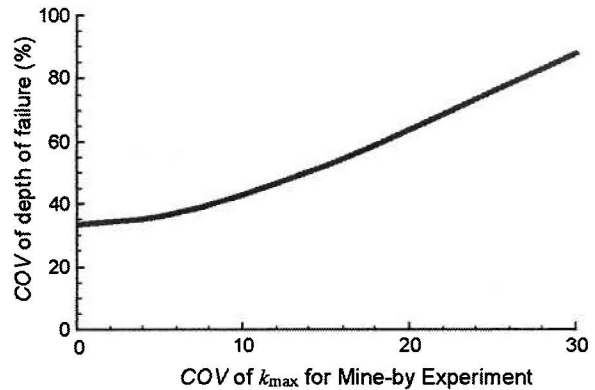


Fig. 29. Relationship between variability in depth of failure and maximum stress ratio  $k_{max}$  for the conditions encountered at the Mine-by Experiment.

$COV = 86\%$ ) is largely due to variability in the rock strength.

For the conditions encountered at the Mine-by Experiment, Fig. 29 illustrates that little can be gained by defining the maximum stress ratio better than with a  $COV$  of about 10%. Hence, if the vertical stress equal to overburden stress (11 MPa) is more or less constant, the horizontal stress ratio should be defined better than  $k_{max} = 5.45 \pm 0.55$  or the horizontal stress better than  $60 \pm 6$  MPa. In other words, more than 10% of measured maximum horizontal stresses would have to

fall outside a range of  $50 < \sigma_H < 70$  MPa before differences in spalling failure could clearly be attributed to stress. Inversely, this analysis demonstrates why it is rather difficult to accurately establish the in situ stress magnitude and stress ratio borehole breakouts.

In summary, while it is demonstrated that the maximum stress near an excavation is sensitive to variations in stress magnitude and stress ratio, it is the variability in rock strength rather than stress, that is responsible for the frequently observed variability in depth of failure and failure mode in general.

## 6. Conclusions

Two forms of instability are readily observed around underground openings: (1) structurally controlled gravity-driven processes leading to wedge type falls-of-ground; and (2) stress-driven failure or yielding.

For the designer, clear guidelines are needed to judge when these conditions are likely to be encountered, particularly during the early stages of a project. While preliminary guidelines are presented in this paper, the designer must be aware that because of the variability of rock mass strength and the in situ stress state that will be encountered, clear boundaries cannot be provided. The procedures outlined in this paper that incorporates this variability are promising. However, these procedures must be incorporated into the overall project risk assessment. In situations where project risks are high in situ stress may have to be measured.

Once a project begins construction, observations can be used to assess tunnel performance against predicted performance using assumed input parameters, a key component of the Observation Design Method. Such back-analysis are essential in deep underground mining where stress levels are elevated due to high extraction ratios and complex tunnel geometries.

A key factor in the analysis of stress-driven instability is that there is no clear definition of acceptable stability or of failure. In practical terms stability is judged to be acceptable when the rock mass deformations are controlled, when the support elements are not over stressed, and when the underground opening is performing as intended. While in situ stress is an important parameter in judging this acceptability, as demonstrated in this paper it is the strength to stress ratio that ultimately determines the stability.

## Acknowledgements

The authors wish to acknowledge the enormous contribution to understanding stress and stress-driven instability made through the research carried out at AECL's Underground Research Laboratory, Canada and SKB's Hard Rock Laboratory, Sweden.

## References

- [1] Peck RB. Ninth rankine lecture: advantages and limitations of the observational method in applied soil mechanics. *Géotechnique* 1969;19(2):171–87.
- [2] Herget G, Arjang B. Update on ground stresses in the Canadian Shield. In: Herget G, Arjang B, Bétournay M, Gyenge M, Vongpaisal S, Yu Y, editors. *Proceedings of the Stresses in Underground Structures*, Ottawa. Ottawa, Canada: Canadian Government Publishing Centre; 1990. p. 33–47.
- [3] Stephansson O. Rock stress in the Fennoscandian Shield. In: Hudson JA. editor. *Comprehensive rock engineering—rock testing and site characterization*, vol. 3. Oxford: Pergamon Press; 1993. p. 445–59.
- [4] Walker JR, Martin CD, Dzik EJ. Confidence intervals for in situ stress measurements. *Int J Rock Mech Min Sci Geomech Abstr* 1990;27(2):139–41.
- [5] Wiles TD, Kaiser PK. A new approach for the statistical treatment of stress tensors. In: Herget G, Arjang B, Bétournay M, Gyenge M, Vongpaisal S, Yu Y, editors. *Proceedings of the Stresses in Underground Structures*, Ottawa. Ottawa, Canada: Canadian Government Publishing Centre; 1990. p. 62–76.
- [6] Martin CD, Read RS, Chandler NA. Does scale influence in situ stress measurements? Some findings at the Underground Research Laboratory. In: da Cunha AP, editor. *Proceedings of the First International Workshop on Scale Effects in Rock Masses*, Loen, Norway. Rotterdam: A.A. Balkema; 1990. p. 307–16.
- [7] Wiles TD, Kaiser PK. In situ stress determination using the under-excavation technique—I. Applications. *Int J Rock Mech Min Sci Geomech Abstr* 1994;31(5):447–56.
- [8] Martin CD, Chandler NA. Stress heterogeneity and geological structures. *Int J Rock Mech Min Sci Geomech Abstr* 1993; 30(7):993–9.
- [9] Christiansson R, Martin CD. In-situ stress profiles with depth from site characterization programs for nuclear waste repositories. In: Särkkä P, Eloranta P, editors. *Proceedings of the EUROCK 2001*, Espoo, Finland. Rotterdam: A.A. Balkema; 2001. p. 737–42.
- [10] Arjang B, Herget G. In situ ground stresses in the Canadian hardrock mines: an update. *Int J Rock Mech Min Sci* 1997; 34(3–4):652.
- [11] Sheorey P. A theory for in situ stresses in isotropic and transversely isotropic rock. *Int J Rock Mech Min Sci Geomech Abstr* 1994;31(1):35–46.
- [12] Hudson JA. Strategy for a rock mechanics site descriptive model: a test case based on data from the Äspö HRL. SKB Technical Report R-02-04, Swedish Nuclear Fuel and Waste Management Company, Stockholm, Sweden, 2002.
- [13] Hoek E, Brown ET. *Underground excavations in rock*. London: The Institution of Mining and Metallurgy; 1980.
- [14] Brady BHG, Brown ET. *Rock Mechanics for underground mining*, 2nd ed. London: Chapman & Hall; 1993. 571p.
- [15] Kaiser PK, Yazici S, Maloney S. Mining-induced stress change and consequences of stress path on excavation stability—a case study. *Int J Rock Mech Min Sci* 2001;38(2):167–80.
- [16] Kaiser PK, Diederichs MS, Martin CD, Sharp J, Steiner W. Keynote: underground works in hard rock tunnelling and mining. In: *Proceedings of the GeoEng2000, An International Conference on Geotechnical and Geological Engineering*, Melbourne, vol. 1: *Invited Papers*. Lancaster: Technomic Publishing Co., Inc; 2000. p. 841–926.
- [17] Eberhardt E. Numerical modelling of three-dimensional stress rotation ahead of an advancing tunnel face. *Int J Rock Mech Min Sci* 2002;38(4):499–518.
- [18] Hoek E, Kaiser PK, Bawden WF. Support of underground excavations in hard rock. Rotterdam: A.A. Balkema; 1995. 215p.

- [19] Hoek E, Marinov P. Predicting tunnel squeezing problems in weak heterogeneous rock masses. Part 1: estimating rock mass strength and Part 2: potential squeezing problems in deep tunnels. *Tunnels and Tunnelling International* 2000, November and December.
- [20] Hoek E, Carranza-Torres C, Corkum B. Hoek–Brown failure criterion—2002 edition. In: Hammah R, Bawden W, Curran J, Telesnicki M. editors. *Proceedings of the Fifth North American Rock Mechanics Symposium and 17th Tunnelling Association of Canada Conference: NARMS-TAC*, vol. 1, Toronto. Toronto: University of Toronto Press; 2002. p. 267–73.
- [21] Deere DU. Geological considerations. In: Stagg KG, Zienkiewicz OC, editors. *Rock mechanics in engineering practice*. London: Wiley; 1980. p. 1–20.
- [22] Muirwood AM. Tunnels for roads and motorways. *Quart J Geol* 1972;5:119–20.
- [23] Adyan O, Akagi T, Kawamoto T. The squeezing potential of rock around tunnels: theory and prediction with examples taken from Japan. *Rock Mech Rock Eng* 1996;29(3):125–43.
- [24] Sakurai S. Displacements measurements associated with the design of underground openings. In: *Proceedings of the International Symposium on Field Measurements in Geomechanics*, vol. 2, Zurich, 1983. p. 1163–78.
- [25] Chern JC, Yu CW, Shiao FY. Tunnelling in squeezing ground and support estimation. In: *Proceedings of the Regional Symposium on Sedimentary Rock Engineering*, Taipei, 1998. p. 293–7.
- [26] Hoek E. Keynote address: tunnel support in weak rock. In: *Proceedings of the Symposium of Sedimentary Rock Engineering*, Taipei, Taiwan, 1998. p. 1–12.
- [27] Hoek E. The thirty sixth Karl Terzaghi lecture: big tunnels in bad rock. *J Geotech Geoenviron Eng* 2001;127(9):726–40.
- [28] Martin CD, Kaiser PK, McCreath DR. Hoek–Brown parameters for predicting the depth of brittle failure around tunnels. *Can Geotech J* 1999;36(1):136–51.
- [29] Aglawe JP. Unstable and violent failure around underground openings in highly stressed ground. PhD thesis, Department of Mining Engineering, Queen's University, Kingston, Canada, 1998.
- [30] Barton N, By TL, Chryssanthakis P, Tunbridge L, Kristiansen J, Løset F, Bhasin RK, Westerdahl H, Vik G. Predicted and measured performance of the 62 m span Norwegian Olympic Ice Hockey Cavern at Gjøvik. *Int J Rock Mech Min Sci Geomech Abstr* 1994;31(6):617–41.
- [31] Mathews KE, Hoek E, Wyllie DC, Stewart SBV. Prediction of stable excavations for mining at depth below 1000 metres in hard rock. *CANMET Report DSS Serial No. OSQ80-00081*, Natural Resources Canada, Ottawa, 1981.
- [32] Potvin Y, Hudyma MR, Miller HDS. Design guidelines for open stope support. *Bull Can Min Metall* 1989;82(926):53–62.
- [33] Alcott JM, Kaiser PK, Gauthier M, Nelson D, Mah P, SHARK: Stability hazard and risk assessment at Placer Dome's Campbell mine. In: *Proceedings of the Colloque de Contrôle de Terrain*, Val-d'Or, 1999. p. 1–9.
- [34] Martin CD, Tannant DD, Yazici S, Kaiser PK. Stress path and instability around mine openings. In: Vouille G, Berest P. editors. *Proceedings of the Ninth, ISRM Congress on Rock Mechanics*, vol. 1. Paris. Rotterdam: A.A. Balkema; 1999. p. 311–5.
- [35] Martin CD, Espley S, Yazici S, Tan G. Using numerical models to quantify stope dilution. In: *CD-ROM Proceedings of the 102nd Canadian Institute of Mining and Metallurgy Annual General Meeting*, Toronto. Montreal: Canadian Institute of Mining and Metallurgy; 2000. p. 1–8.
- [36] Diederichs MS, Kaiser PK. Tensile strength and abutment relaxation as failure control mechanisms in underground excavations. *Int J Rock Mech Min Sci* 1999;36(1):69–96.
- [37] Kaiser PK, Yazici S, Nosé J. Effect of stress change on the bond strength of fully grouted cables. *Int J Rock Mech Min Sci Geomech Abstr* 1992;29(3):293–306.
- [38] Harr ME. *Reliability-based design in civil engineering*. New York: McGraw-Hill; 1987.
- [39] Hoek E. A limit equilibrium analysis of surface crown pillar stability. In: Bétournay MC. editor. *Proceedings of the Surface Crown Pillar Evaluation for Active and Abandoned Metal Mines*, Timmons. Ottawa: Canadian Government Publishing Centre; 1989. p. 3–13.
- [40] Pine RJ. Risk analysis design applications in mining geomechanics. *Trans Institut Min and Metal (Section A: Mining industry)* 1992;101:149–58.
- [41] Martin CD, Read RS. AECL's mine-by experiment: a test tunnel in brittle rock. In: Aubertin M, Hassani F, Mitri H, editors. *Proceedings of the Second North American Rock Mechanics Symposium*, vol. 1, Montreal. Rotterdam: A.A. Balkema; 1996. p. 13–24.
- [42] Martin CD. Characterizing in situ stress domains at the AECL underground research laboratory. *Can Geotech J* 1990;27:631–46.
- [43] Serafim JL, Pereira JP. Considerations of the geomechanical classification of Bieniawski. In: *Proceedings of the International Symposium on Engineering Geology and Underground Construction*, vol. 1, Lisbon, 1983. p. II.33–42.
- [44] Bieniawski ZT. Determining rock mass deformability: experience from case histories. *Int J Rock Mech Min Sci Geomech Abstr* 1978;15:237–47.
- [45] Martin CD, Read RS, Lang PA. Seven years of in situ stress measurements at the URL—an overview. In: Hustrulid W, Johnson G. editors. *Proceedings of the 31st US Symposium on Rock Mechanics*, Golden. Rotterdam: A.A. Balkema; 1990. p. 15–25.
- [46] Martin CD, Chandler NA, Read RS. The role of convergence measurements in characterizing a rock mass. *Can Geotech J* 1996;33(2):363–70.
- [47] Read RS. Interpreting excavation-induced displacements around a tunnel in highly stressed granite. PhD thesis, Department of Civil & Geological Engineering, University of Manitoba, Winnipeg, Manitoba, Canada, 1994.
- [48] Hedley DGF, Grant F. Stope-and-pillar design for the Elliot Lake uranium mines. *Bull Can Inst Min Metall* 1972;65:37–44.
- [49] Herget G. Ground stress determinations in Canada. *Rock Mech Rock Eng* 1974;10(3–4):37–51.
- [50] Brown ET, Hoek E. Trends in relationships between measured and in situ stresses and depth. *Int J Rock Mech Min Sci Geomech Abstr* 1978;15:211–5.
- [51] McGarr A. State of stress in the earth's crust. *Ann Rev Earth Planet Sci* 1978;6:405–36.
- [52] Herget G. Stress assumptions for underground excavations in the Canadian Shield. *Int J Rock Mech Min Sci Geomech Abstr* 1987;24(1):95–7.
- [53] Arjang B. Pre-mining stresses at some hard-rock mines in the Canadian Shield. In: *Proceedings of the 30th US Symposium on Rock Mechanics*, Morgentown. Rotterdam: A.A. Balkema; 1989. p. 545–51.
- [54] Herget G. Rock stresses and rock stress monitoring in Canada. In: Hudson JA. editor. *Comprehensive rock engineering—rock testing and site characterization*, vol. 3. Oxford: Pergamon Press; 1993. p. 473–96.
- [55] Andersson J, Ljunggren C. A geostatistical approach to evaluate differences in results between hydraulic fracturing and overcoring. In: Sugawara K, Obara Y, editors. *Proceedings of the International Symposium on Rock Stress*, Kumamoto. Rotterdam: A.A. Balkema; 1997. p. 223–7.
- [56] Batchelor AS, Kwakwa KA, Proughten AJ, Davies N. Determination of the in-situ stresses at Sellafeld, UK: a case study. In: Sugawara K, Obara Y, editors. *Proceedings of the International Symposium on Rock Stress*, Kumamoto. Rotterdam: A.A. Balkema; 1997. p. 265–76.